PLOS Pathogens

RESEARCH ARTICLE

Rev-RRE activity modulates HIV-1 replication and latency reactivation: Implications for viral persistence and cure strategies

Godfrey A. Dzhivhuho[1,2☯], Patrick E. H. Jackson[2,3☯], Ethan S. Honeycutt[1,2¤a], Flavio da Silva Mesquita[1¤b], Jing Huang[1], Marie-Louise Hammarskjold[1,2], David Rekosh[1,2*]

1 Department of Microbiology, Immunology, and Cancer Biology, School of Medicine, University of Virginia, Charlottesville, Virginia, United States of America, **2** Myles H. Thaler Center for HIV and Human Retrovirus Research, University of Virginia, Charlottesville, Virginia, United States of America, **3** Division of Infectious Diseases and International Health, Department of Medicine, School of Medicine, University of Virginia, Charlottesville, Virginia, United States of America

☯ These authors contributed equally to this work.
¤a Current address: Department of Molecular Biology and Microbiology, Case Western Reserve University, Cleveland, Ohio, USA
¤b Current address: Virology Program, Harvard University Medical School, Boston, Massachusetts, USA
* dr4u@virginia.edu

Citation: Dzhivhuho GA, Jackson PEH, Honeycutt ES, Mesquita F da S, Huang J, Hammarskjold M-L, et al. (2025) Rev-RRE activity modulates HIV-1 replication and latency reactivation: Implications for viral persistence and cure strategies. PLoS Pathog 21(5): e1012885. https://doi.org/10.1371/journal.ppat.1012885

Editor: Li Wu, University of Iowa, UNITED STATES OF AMERICA

Received: January 3, 2025

Accepted: April 11, 2025

Published: May 15, 2025

Data availability statement: All relevant data are within the manuscript and its Supporting Information files.

Funding: The flow cytometry data for this manuscript were generated at the University

Abstract

The HIV-1 Rev-RRE regulatory axis plays a crucial role in viral replication by facilitating the nucleo-cytoplasmic export and expression of viral mRNAs with retained introns. In this study, we investigated the impact of variation in Rev-RRE functional activity on HIV-1 replication kinetics and reactivation from latency. Using a novel HIV-1 viral vector with an interchangeable Rev cassette, we engineered viruses with two diverse Rev functional activities and demonstrated that higher Rev-RRE activity confers greater viral replication capacity while maintaining a constant level of Nef expression. In addition, a low Rev activity virus rapidly acquired a compensatory mutation in the RRE that significantly increased Rev-RRE activity and replication. In a latency model, proviruses with differing Rev-RRE activity levels varied in the efficiency of viral reactivation, affecting both initial viral release and subsequent replication kinetics. These results demonstrate that activity differences in the Rev-RRE axis among different viral isolates have important implications for HIV replication dynamics and persistence. Importantly, our findings indicate that bolstering Rev/RRE activity could be explored as part of latency reversal strategies in HIV cure efforts.

of Virginia Flow Cytometry Core Facility (RRid:SCR_017829), with partial support from the NCI Cancer Center Grant (P30-CA044579, D.R. and M.-L H). Partial salary support was provided by the Myles H. Thaler Endowed Professorship (D.R.) at the University of Virginia, the Charles Ross Jr Endowed Professorship (M.-L. H) at the University of Virginia, and NIH grant K08 AI136671 (P.E.H.J). Research support was provided by Myles H. Thaler Research Support Gift at the University of Virginia (D.R. and M.-L. H.) and NIH grant R21 AI134208 (D.R. and M.-L. H.). The funders had no role in study design, data collection and analysis, decision to publish, or preparation of the manuscript.

Competing interests: The authors have declared that no competing interests exist

Author summary

The activity of the HIV-1 Rev-RRE axis is essential for viral replication and varies among primary viral isolates. However, the role of this for viral fitness, evolution, and persistence has not previously been investigated. Our results show that during *in vitro* replication, there is a selective fitness advantage for a virus with higher Rev-RRE activity and that HIV has the ability to fine-tune this regulatory system with minimal sequence changes. Additionally, the maintenance of Nef expression in a low Rev activity virus suggests a potential mechanism for balancing immune evasion and replication capacity in different selection landscapes within a host. We also show that the virus with low Rev-RRE activity was more difficult to reverse from latency than the virus with higher Rev-RRE activity. Thus, differences in provirus Rev-RRE activity may be a barrier to developing effective latency reversal strategies. These findings provide new insights into the complex roles the Rev/RRE axis plays in functionality, viral fitness, evolution, and persistence.

Introduction

Retroviruses have compact genomes and utilize a complex alternative splicing pattern to express the full range of viral mRNAs required for replication. As a result of this strategy, viral RNAs with retained introns (IR-mRNAs) have to be exported from the cell nucleus to the cytoplasm for genome packaging into new virus particles and for the production of structural proteins. Retroviruses use one of two strategies to overcome the normal cellular restrictions to export of these RNAs. “Simple” retroviruses, such as the Mason-Pfizer Monkey Virus, contain an RNA structure in the IR-mRNAs, the CTE [1], that directly recruits the cellular factors Nxf1 and Nxt1 to permit nuclear export. In contrast, “complex” retroviruses require both a structured element in the IR-mRNAs and a viral regulatory protein, to accomplish this task [2].

HIV-1 is a complex retrovirus that utilizes the viral protein Rev, and an RNA structure known as the Rev Response Element (RRE), to export its viral IR-mRNAs [3–5]. Rev is translated from a completely spliced mRNA and is imported into the nucleus, where it binds to the RRE present in the unspliced and incompletely spliced viral mRNAs. Rev then acts as an adapter on the RRE to recruit cellular factors including Crm1 and RanGTP. This creates a complex that enables the export of the IR-mRNA to the cytoplasm [6–11].

The RRE of the lab isolate pNL4–3, which is used in many *in vitro* studies, is a highly structured element of about 350 nucleotides [12]. The element exists in a dynamic equilibrium between two low-energy conformations containing either four or five stem loops [13]. The highest affinity binding site for Rev is located on stem-loop IIB, and a complex of about six to eight Rev monomers sequentially assembles on the RRE [14]. As with all other regions of the HIV genome, the RRE is subject to frequent mutations, resulting in sequence differences among primary isolates. We previously observed the sequence, structural, and functional evolution of the RRE

in circulating viral variants in individuals over time [15,16]. A small number of nucleotide changes was sufficient to cause a substantial alteration in RRE secondary structure, as well as significant differences in Rev-RRE functional activity [16]. Previous studies have also shown that one or two changes in the RRE allows the virus to escape inhibition by small molecules or a trans-dominant negative Rev protein [17,18].

The Rev protein is also subject to significant sequence and functional variation. The prototypical (subtype B) Rev consists of 116 amino acids and includes a bipartite oligomerization domain [19], a nuclear export signal [20], and an arginine-rich motif, which serves as both the RNA binding region and the nuclear localization signal [21,22]. We previously described two subtype G Revs from primary isolates that showed widely disparate activity levels [23]. The high activity, 9-G, and low activity, 8-G, Rev sequences differed at 29 amino acid positions. However, the activity difference between the two Rev proteins was subsequently shown to be attributable to two single amino acid differences in the first oligomerization domain [24].

HIV replication is dependent on a functional Rev-RRE axis, but the functional plasticity of Rev and the RRE permits fine-tuning of Rev-RRE activity through small sequence changes in either element. The consequences of this variation for HIV pathogenesis have not been fully explored. However, in another complex retrovirus, Equine Infectious Anemia Virus (EIAV), variations in the Rev-RRE axis over time are clearly associated with clinical disease progression [25–27]. In the case of HIV, Rev activity has been shown to be a determinant of the sensitivity of HIV-1-infected primary T cells to cytotoxic T-lymphocyte killing [28] and RRE activity has been positively correlated with the rate of CD4 count decline [29,30]. Rev-RRE activity has also been shown to affect the fitness of viral variants in the context of female-to-male sexual transmission [31]. Thus, it is reasonable to hypothesize that Rev-RRE activity differences may play a role in many aspects of HIV pathogenesis, including in the dynamics of the reservoir and viral rebound after treatment interruption. In this study, we explored the effect of Rev-RRE activity differences on viral replication kinetics and *in vitro* fitness in the context of both a spreading infection and reactivation from latency. We focused on two subtype G Rev variants, with widely different activities, to provide proof of concept that establishes the consequences of Rev-RRE variation on these processes.

Results

Construction and characterization of an HIV proviral construct with an interchangeable Rev

The coding region of the HIV Rev gene overlaps the coding regions of both Env and Tat. Thus, to investigate the impact of variation in Rev activity on viral replication kinetics, it was essential to create an infectious construct that relocated Rev into a position where it could be manipulated without changing other HIV genes. To do this, we first silenced Rev in the pNL4–3 proviral clone by mutating the AUG initiation codon to ACG and the 23rd codon, UAU, to a stop codon, UAA. The stop codon in Rev introduced a conservative serine to threonine change at amino acid position 70 in the overlapping Tat open reading frame (Fig 1A). We then inserted a cassette upstream of Nef that contained a cDNA copy of NL4–3 Rev, followed by an internal ribosomal entry site (IRES). This allowed both Rev and Nef to be expressed from a fully spliced HIV mRNA that would normally encode only Nef.

Another important feature of this construct is that the Rev sequence is flanked by restriction enzyme sites, so that it can easily be exchanged for alternative Rev sequences. This allowed us to make two additional constructs using sequences from two Rev variants (8-G, accession FJ389367; 9-G, accession JX140676). The 8-G and 9-G Rev proteins were previously shown to have disparate functional activities. When tested on the NL4–3 RRE, the functional activity of these Revs differed by 4–5-fold [23]. The new proviral clones were named pNLRev_IRES_Nef (HamRek archive #5833), p8-GRev_IRES_Nef (HamRek archive #5830) and p9-GRev_IRES_Nef (HamRek archive #5831).

To analyze how moving Rev to a different region affected replication and Nef expression, we first transfected 293T cells with pNLRev_IRES_Nef and the original pNL4–3 proviral clone. Forty-eight hours (48h) after transfection, supernatants were collected and assayed for p24 (S1B Fig). One hundred nanograms of supernatant p24 were then used to infect

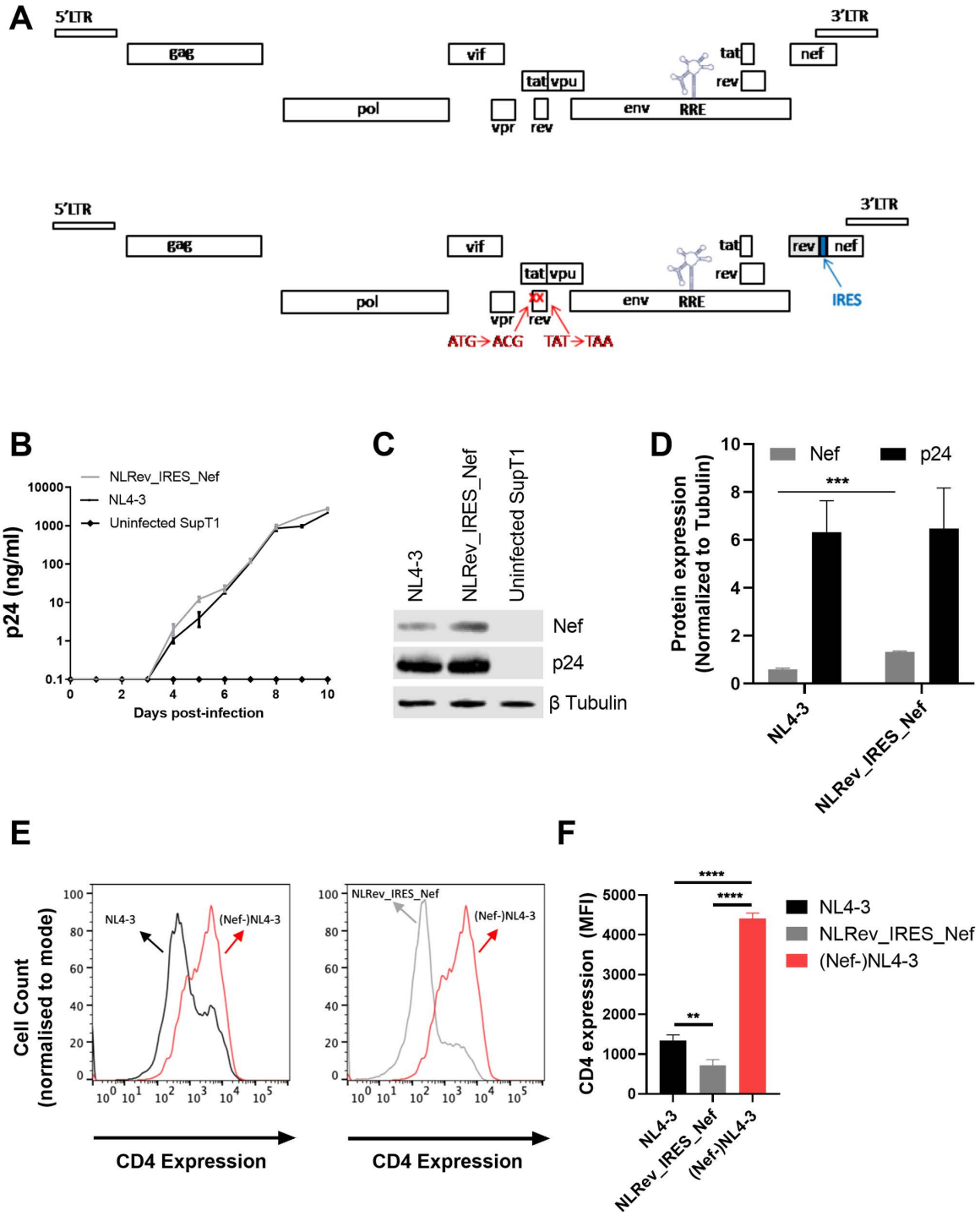

Fig 1. Construction and characterization of an HIV proviral clone with an interchangeable *rev* gene. (A) Schematic of HIV proviral constructs. Upper panel: original NL4-3. Lower panel: modified NLRev_IRES_Nef. The native *rev* gene was silenced by start codon mutation (AUG to ACG) and stop codon introduction at position 23 (UAC to UAA). An NL4-3 *rev* cDNA cassette with an IRES was inserted upstream of *nef*, flanked by restriction sites for easy exchange. **(B)** SupT1 cells were infected with NL4-3 (black line) and NLRev_IRES_Nef (grey line) viruses at an MOI of 0.005. Viral replication was monitored by p24 ELISA of culture supernatants over time. **(C)** Representative Western blot analysis of p24 and Nef expression in SupT1 cells infected with NL4-3 or NLRev_IRES_Nef viruses at day 8 post-infection. Beta-tubulin was used as a loading control. **(D)** Quantification of Nef (grey bar) and p24 (black bar) expression from Western blot analysis. **(E)** Overlaid histograms of CD4 expression in SupT1 cells infected (day 8) with

NL4-3 (black), NLRev_IRES_Nef (gray), or a Nef-negative NL4-3 control (red). Histograms are gated on p24$^+$ cells, demonstrating the relative reduction in CD4 surface levels. **(F)** Quantification of CD4 downmodulation from **(E)**. Bars represent mean ± SD from three independent experiments. Statistical significance was determined by an unpaired, two-tailed t-test with FDR correction (**$p < 0.01$, ***$p < 0.001$, ****$p < 0.0001$). Error bars in (B) represent mean ± SEM of three independent experiments, while error bars in (D) and (F) represent mean ± SD of three independent experiments.

https://doi.org/10.1371/journal.ppat.1012885.g001

SupT1 cells (1x10^6/ml), creating intermediate viral stocks (S1C Fig). These viral stocks were passaged a second time in SupT1 cells (S1D Fig), creating the final expanded viral stocks whose titers were determined by $TCID_{50}$. The details of this procedure are shown in S1A Fig and further described in materials and methods. We first compared the replication kinetics of the two viruses. To do this, parallel cultures of SupT1 cells were infected with both viruses at a multiplicity of infection (MOI) of 0.005. Viral replication was assessed by measuring the levels of p24 in culture supernatants over time. As can be seen in Fig 1B, these viruses replicated similarly as measured by p24 production.

To analyze Nef expression, cells were collected eight days post-infection and subjected to Western blot analysis. Whereas the levels of p24 were comparable between the two viruses, the NLRev_IRES_Nef virus appeared to express higher levels of Nef compared to NL4–3 (Fig 1C and 1D). This could be due to Nef expression from both spliced and unspliced mRNA in the engineered construct because of the presence of an IRES.

We next assessed Nef functionality in these two viruses. HIV Nef downregulates cell surface CD4 expression through clathrin- and adaptor protein complex 2-dependent endocytosis [32,33]. SupT1 cells were infected with NL4–3 or NLRev_IRES_Nef viruses at an MOI of 0.005 and then stained for intracellular p24 and surface CD4 expression at day 8 post-infection. Cells infected with a Nef-negative NL4–3 virus were used as a control. Both NL4–3 and NLRev_IRES_Nef-infected cells displayed downmodulation of CD4 compared to the Nef-negative control, demonstrating that the modified viruses express a functional Nef protein (Fig 1E). However, quantitative analysis (Fig 1F) revealed that cells infected with NLRev_IRES_Nef showed a significantly greater reduction in surface CD4 than did cells infected with wild-type NL4–3. This enhanced CD4 downmodulation is consistent with the higher Nef expression detected in NLRev_IRES_Nef-infected cells.

Taken together the results of these experiments indicate that the relocation of Rev and the incidental change in Tat did not impair viral replication kinetics or the ability of the virus to produce a functional Nef protein.

A virus with low Rev functional activity replicates poorly compared to a virus with high Rev functional activity

We next examined the replication kinetics of the 8-GRev_IRES_Nef and 9-GRev_IRES_Nef viruses in comparison with NLRev_IRES_Nef. To do this, SupT1 cells were infected with each virus from the expanded stocks at an equal MOI (0.005). Measurement of p24 in culture supernatants by ELISA revealed that the 9-GRev_IRES_Nef virus replicated similarly to the NLRev_IRES_Nef virus. However, the 8-GRev_IRES_Nef virus replicated much less efficiently (Fig 2A). To verify that the observed replication differences were not restricted to the SupT1 cell line, we also infected PHA/IL-2–activated primary CD4$^+$ T cells with 8-GRev_IRES_Nef or 9-GRev_IRES_Nef, at an MOI of 0.05, using the same spin-oculation protocol. Viral replication was then monitored by p24 ELISA on culture supernatants collected every 3–4 days. Similar to our findings in SupT1 cells, 9-GRev_IRES_Nef replicated more efficiently than 8-GRev_IRES_Nef (S2 Fig). These data confirm that the slower replication kinetics of 8-GRev_IRES_Nef are not cell-line specific, reinforcing the conclusion that variation in Rev-RRE functional activity strongly influences HIV-1 replication capacity. Levels of Nef and p24 in the infected cells were also measured by western blot analysis. Although there was no difference in Nef expression, p24 levels were much lower in cells infected with the 8-GRev_IRES_Nef virus compared to those infected with NL4Rev-IRES-Nef or 9-GRev_IRES_Nef viruses. The 9-GRev_IRES_Nef virus exhibited the highest p24 expression (Fig 2B and 2C). For both p24 and Nef, statistical comparisons of band intensities were conducted using an unpaired t-test with FDR correction.

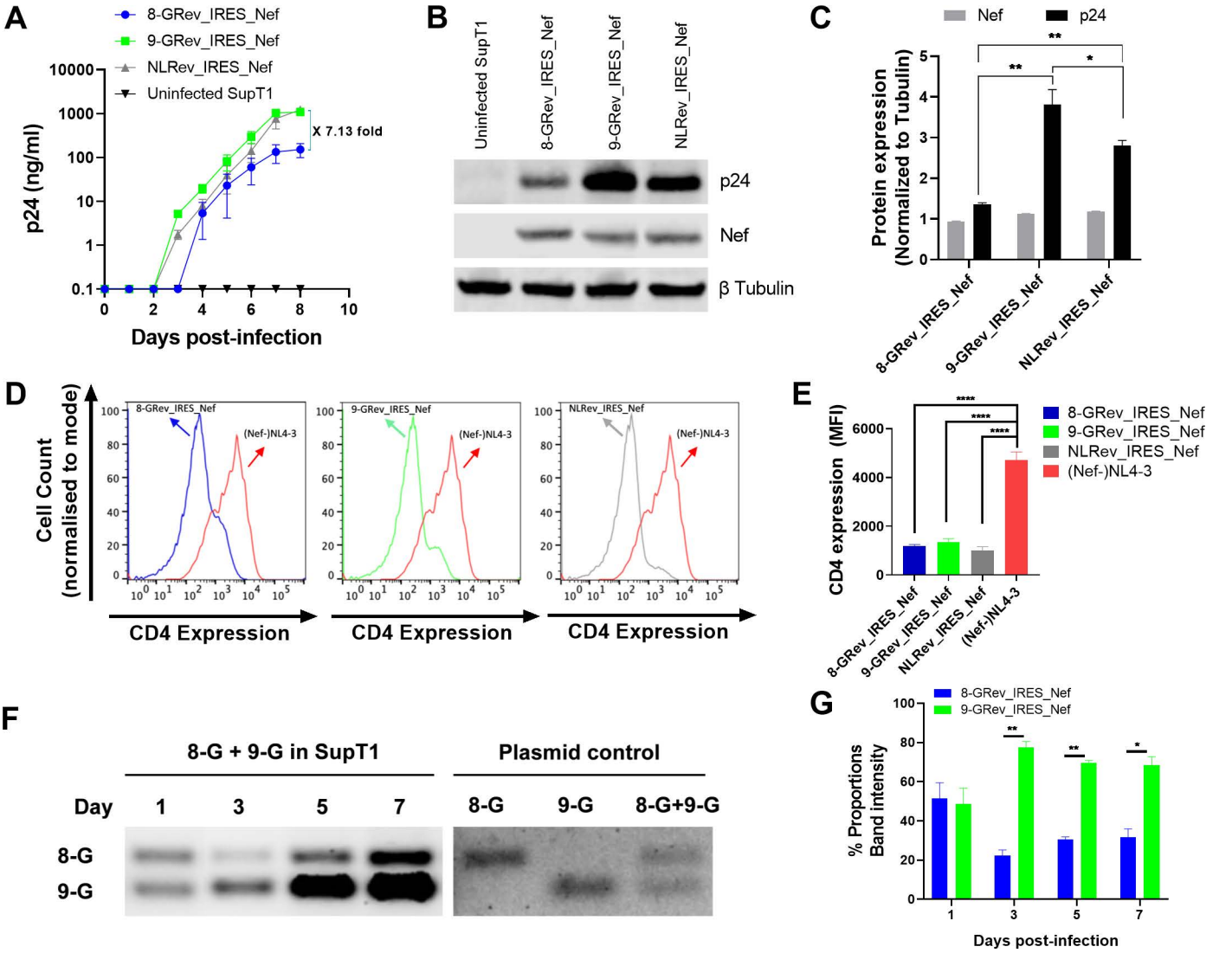

Fig 2. Viruses with low Rev functional activity replicate poorly compared to viruses with high Rev functional activity. (A) SupT1 cells were infected with 8-GRev_IRES_Nef (low Rev activity) (blue), 9-GRev_IRES_Nef (high Rev activity) (green), and NLRev_IRES_Nef (control) (grey) viruses at an MOI of 0.005. Viral replication was assessed by p24 ELISA of culture supernatants over time. (B) Western blot analysis of Nef and p24 expression in infected cells at day 8 post-infection. Beta-tubulin was used as a loading control. (C) Quantification of Nef and p24 expression from Western blot analysis in B, normalized to beta-tubulin. (D) Histograms of CD4 expression on SupT1 cells (day 8) infected with 8-GRev_IRES_Nef, 9-GRev_IRES_Nef, or NLRev_IRES_Nef, compared to a Nef-negative NL4–3 control. (E) Quantification of CD4 downmodulation from (D), relative to the Nef-negative control. (F) SupT1 cells were co-infected with 8-GRev_IRES_Nef and 9-GRev_IRES_Nef viruses at an MOI of 0.005 each. Left panel: Representative gel image showing PCR products of cellular DNA targeting Rev at days 1, 3, 5, and 7 post-infection. Right panel: PCR plasmid controls. (G) Quantification of relative proviral DNA levels from the competition assay. Bars represent the ratio of 9-GRev_IRES_Nef to 8-GRev_IRES_Nef proviral DNA at each time point. Error bars in (A) represent mean ± SEM of three independent experiments, while those in (C), (E), and (G) represent mean ± SD of three independent experiments. Statistical significance was calculated using an unpaired, two-tailed t-test with FDR correction (*$p < 0.05$, **$p < 0.01$, ***$p < 0.001$, ****$p < 0.0001$).

https://doi.org/10.1371/journal.ppat.1012885.g002

To determine whether Nef function was affected, the ability of each virus to downmodulate CD4 was tested. Flow cytometry of p24-stained cells revealed that all viruses, including the 8-GRev_IRES_Nef virus, downmodulated CD4 compared to the Nef-negative NL4–3 control (Fig 2D and 2E), showing that all the viruses expressed functional Nef.

To directly compare the replicative fitness of viruses with low (8-GRev_IRES_Nef) and high (9-GRev_IRES_Nef) Rev activity, a competition assay was performed by co-infecting SupT1 cells with both viruses. An MOI of 0.005 was used to ensure that the number of co-infected cells would be minimal and thus allow the activity of each Rev to be assessed in parallel. Cellular DNA was collected, and PCR was performed using primers targeting Rev, since the PCR products from the 8-GRev_IRES_Nef and 9-GRev_IRES_Nef viruses are distinguishable by size.

On day 1 both 8-GRev_IRES_Nef and 9-GRev_IRES_Nef proviruses were present in equal amounts, confirming the equal MOI used for infection (Fig 2F and 2G). On days 3, 5, and 7, a significantly higher number of proviral copies of the 9-GRev_IRES_Nef provirus were present in the co-infected cells, demonstrating that the high Rev activity virus outcompeted the low Rev activity virus over time.

Continued passage of the low Rev activity 8-GRev_IRES_Nef virus selected for a single nucleotide change in the RRE

When we continued the infections shown in Fig 2A beyond day 8, we observed a dramatic increase in p24 production in cells infected with the 8-GRev_IRES_Nef virus (Fig 3A). We reasoned that this could be due to the selection of a viral mutant that replicated more efficiently. To examine this, both the RRE and Rev regions of integrated proviruses at the day 10 timepoint were amplified by nested PCR and sequenced using Sanger sequencing. No changes were observed in the Rev sequence (S1 File). However, sequencing of the RRE from 8-GRev_IRES_Nef infected cells revealed that a considerable fraction of the proviruses displayed a single nucleotide change in the stem IIB region of the RRE (Fig 3B) at pNL4–3 residue 7214 (NL4–3 accession number U26942). Sequencing of proviral DNA from the day 6 cells also revealed the same change. In contrast, only negligible amounts of the C7214T mutation were found in proviral DNA from the day 1 cells. In addition, the mutation was completely missing in the proviruses present in the originally infected day 8 cells, the supernatant of which contributed to the viral stock used for the subsequent infection (Fig 3C). The C7214T mutation was also not observed in proviruses sequenced from the 9-GRev_IRES_Nef virus cultures at any of the time points examined (Fig 3A and 3C). Importantly, we also verified the genetic stability of our engineered stop codon and mutated start codon in the original rev reading frame by sequencing proviral DNA from day 10 infections of all three viruses (8-GRev_IRES_Nef, 9-GRev_IRES_Nef, and NLRev_IRES_Nef). No reversion of the introduced stop (UAA) or mutated start codon (ACG) was detected, confirming that the enhanced replication of the 8-GRev_IRES_Nef virus at later time points was driven by the newly acquired C7214T change in the RRE, rather than reversions of our engineered modifications (S3 Fig).

These results suggest that the C7214T change in the RRE of the 8-GRev_IRES_Nef virus, which weakened base pairing in an important region of the RRE, was selected during viral passaging because it promoted Rev-RRE function and thus enhanced replication.

The C7214T mutation in the RRE enhances Rev-RRE dependent viral gene expression and viral replication

Since the RRE overlaps the coding region of Env, the C7214T mutation also introduced a nonsynonymous change of an alanine to a valine in gp41 (A539V). It was therefore of interest to verify that the C7214T mutation resulted in enhanced RRE function independent of a potential effect of the change in Env.

To investigate this, a fluorescence-based assay of Rev-RRE function that we have previously described was used [35]. Briefly, the assay system utilizes an HIV reporter construct derived from NL4–3. This reporter contains an RRE, but does not express a functional Rev. It also contains a sequence encoding GFP inserted into the *gag* region and a sequence encoding mCherry inserted into the *nef* region. Since the GFP sequence is only present in unspliced mRNA, its expression is completely dependent on Rev-RRE activity. However, since mCherry is made from a completely spliced mRNA, its expression is Rev-RRE-independent. Additionally, the RRE in this reporter is flanked by restriction enzyme sites, allowing for easy replacement. Rev can be delivered in *trans* and Rev-RRE activity is then quantified by determining the mean fluorescence intensity of GFP in mCherry positive cells using flow cytometry.

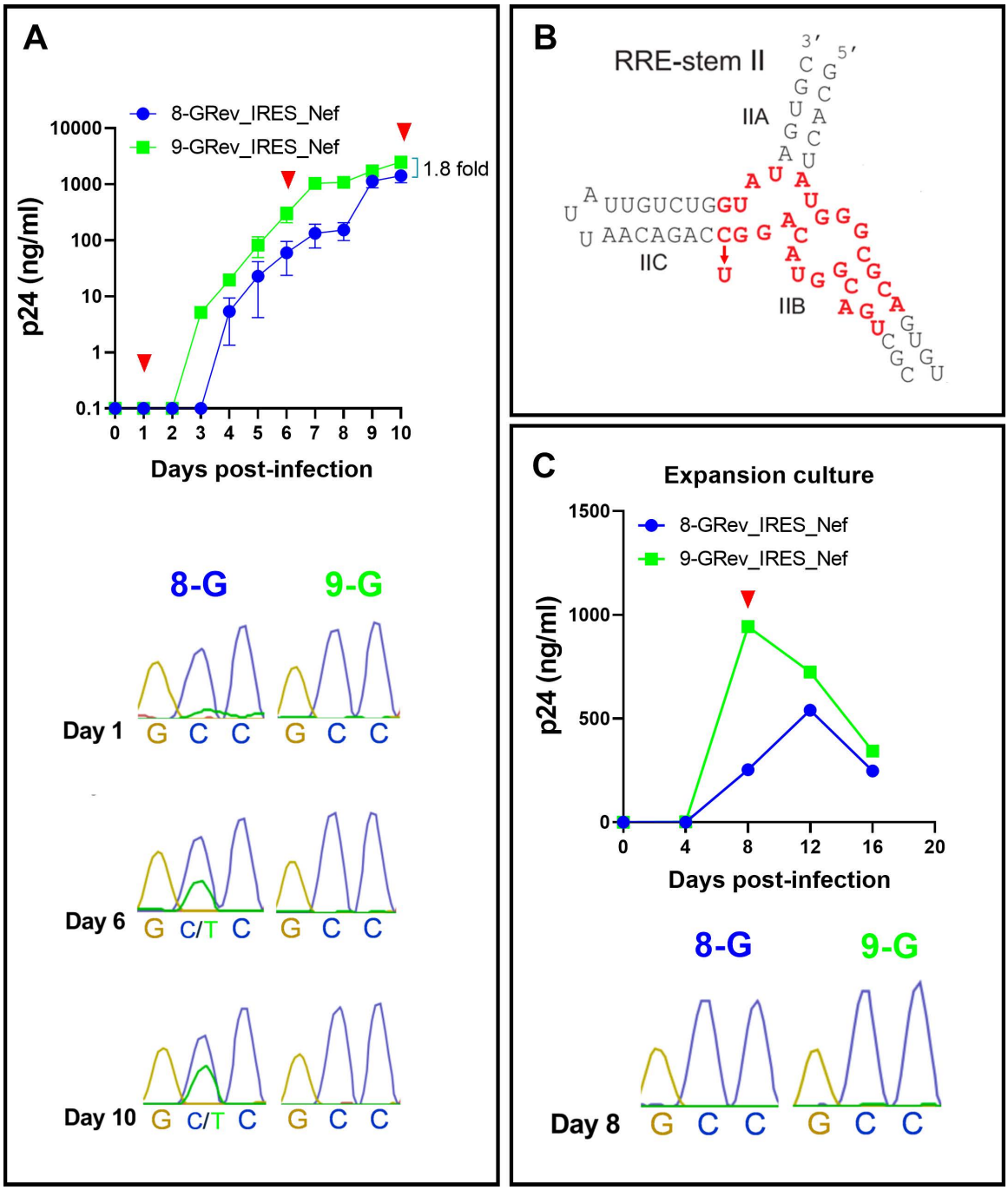

Fig 3. Extended passage of the low Rev activity 8-GRev_IRES_Nef virus selects for a single nucleotide change in the RRE that enhances viral replication. (A) Extended replication kinetics of 8-GRev_IRES_Nef and 9-GRev_IRES_Nef viruses in SupT1 cells. Top: Replication curve showing p24 levels measured by ELISA over time. Red arrows indicate timepoints when the RRE was sequenced from the culture cells. Bottom: Sanger sequencing chromatograms of the RRE region from infected cells at days 1, 6, and 10 post-infection, revealing the emergence of the C7214T mutation. (B) Schematic representation of the HIV-1 RRE stem II region, highlighting the location of the C7214T mutation observed in the 8-GRev_IRES_Nef virus. This figure is adapted from Jayaraman et al. [34], (Fig 1—figure supplement 1B; https://doi.org/10.7554/eLife.04120.004) under the CC BY 4.0 license. The binding site of Rev is highlighted in red, and an arrow showing the position of the C7214T mutation has been added. (C) Characterization of the viral expansion stock. Top: Growth curve of the viral expansion stock in SupT1 cells, showing p24 levels measured by ELISA for 8-GRev_IRES_Nef and 9-GRev_IRES_Nef viruses. Bottom: Sanger sequencing chromatograms of the RRE region from SupT1 bulk culture cells used to produce viral

expansion stocks at day 8 post-infection. Error bars in growth curves represent mean ± SEM of three independent experiments. Sequencing chromatograms are representative of three independent experiments.

https://doi.org/10.1371/journal.ppat.1012885.g003

Reporter constructs containing either the native NL4–3 RRE or the C7214T mutant RRE were constructed, along with plasmids expressing 8-G or 9-G Rev variants. In parallel experiments, the reporter plasmids were then transfected into 293T cells together with varying amounts of the 8-G Rev (Fig 4A) or 9-G Rev plasmids (Fig 4B), and the mean fluorescence intensity (MFI) of GFP was determined. For both Rev proteins, linear dose-response curves were observed. Significantly greater activity was seen with the C7214T mutant RRE compared to the original NL4–3 RRE in conjunction with both 8-G and 9-G Rev proteins, but the increase was more pronounced when 8-G Rev was expressed. This confirmed that the RRE with the C7214T mutation showed higher Rev-RRE activity, particularly in conjunction with 8-G Rev. This strengthens the notion that the mutant was selected because of higher Rev-RRE activity in the resulting 8G-Rev virus.

To directly assess the effect of the RRE mutation on replication kinetics, two new proviral constructs were created, introducing the C7214T mutation into both the RRE of 8-GRev_IRES_Nef (HamRek archive #6468), and 9-GRev_IRES_Nef (HamRek archive #6470) constructs. The plasmids were transfected into 293T cells to produce viral stocks, and the resulting viruses, together with the original 8-GRev_IRES_Nef, and 9-GRev_IRES_Nef viruses, were used to infect SupT1 cells. The results showed that introducing the C7214T mutation in the RRE of the 8-GRev_IRES_Nef virus greatly enhanced replication (Fig 4C), so that it now replicated better than the 9-GRev_IRES_Nef virus (Fig 4E). In contrast, this mutation had only a modest effect on the replication of the 9-GRev_IRES_Nef virus (Fig 4D). These results provide further evidence for the hypothesis that the single RRE nucleotide change was selected since it allowed increased replication of a virus expressing a Rev protein with low activity.

The high Rev-RRE activity virus exhibits enhanced reactivation from latency and viral release compared to the low Rev-RRE activity virus

Finally, we investigated the effect of different levels of Rev-RRE activity on viral reactivation from latency using a model previously described by Lewin, with some modifications (see Methods) (Fig 5A). Prior to infection, we verified that CCL19-treated CD4 + T cells exhibited minimal expression of CD69 and CD25, confirming a resting phenotype, whereas cells treated with phytohaemagglutinin (PHA) and interleukin-2 (IL-2) for 24 hours showed robust upregulation of both markers (S4 Fig). These data confirm that our CCL19-treated cells remained quiescent before viral exposure and that PHA/IL-2 potently activated the cells as intended for subsequent latency reactivation experiments.

We then infected parallel cultures of resting primary CD4 + T cells (verified above) with either the 9-GRev_IRES_Nef, 8-GRev_IRES_Nef, or NLRev_IRES_Nef viruses, at an equal MOI (Fig 5A). Successful equal infection was confirmed by measuring integrated provirus in cells at 24 hours post-infection (Fig 5B). On day three post-infection, cells were divided into two groups that were either treated with the combination of PHA/IL-2 latency reversing agents (LRA) or left untreated. Culture supernatants were collected through day 17 post-infection and analyzed for p24 production, as measured by ELISA.

Following LRA treatment, cells infected with the high Rev-RRE activity virus, 9-GRev_IRES_Nef, produced p24 more rapidly and at a higher rate than cells infected with the low Rev-RRE activity 8-GRev_IRES_Nef virus (Fig 5C). The NLRev_IRES_Nef virus exhibited an intermediate behavior. As expected, cells infected with these viruses without LRA treatment, did not produce detectable p24.

To confirm the presence of integrated virus in the cells that were not reactivated, a semi-nested Alu-gag PCR followed by LTR-RU5 amplification of the first-round PCR product was performed using genomic DNA. This confirmed that the cells were infected and contained integrated proviral DNA and that the state of latency was maintained in the absence the LRA (Fig 5D).

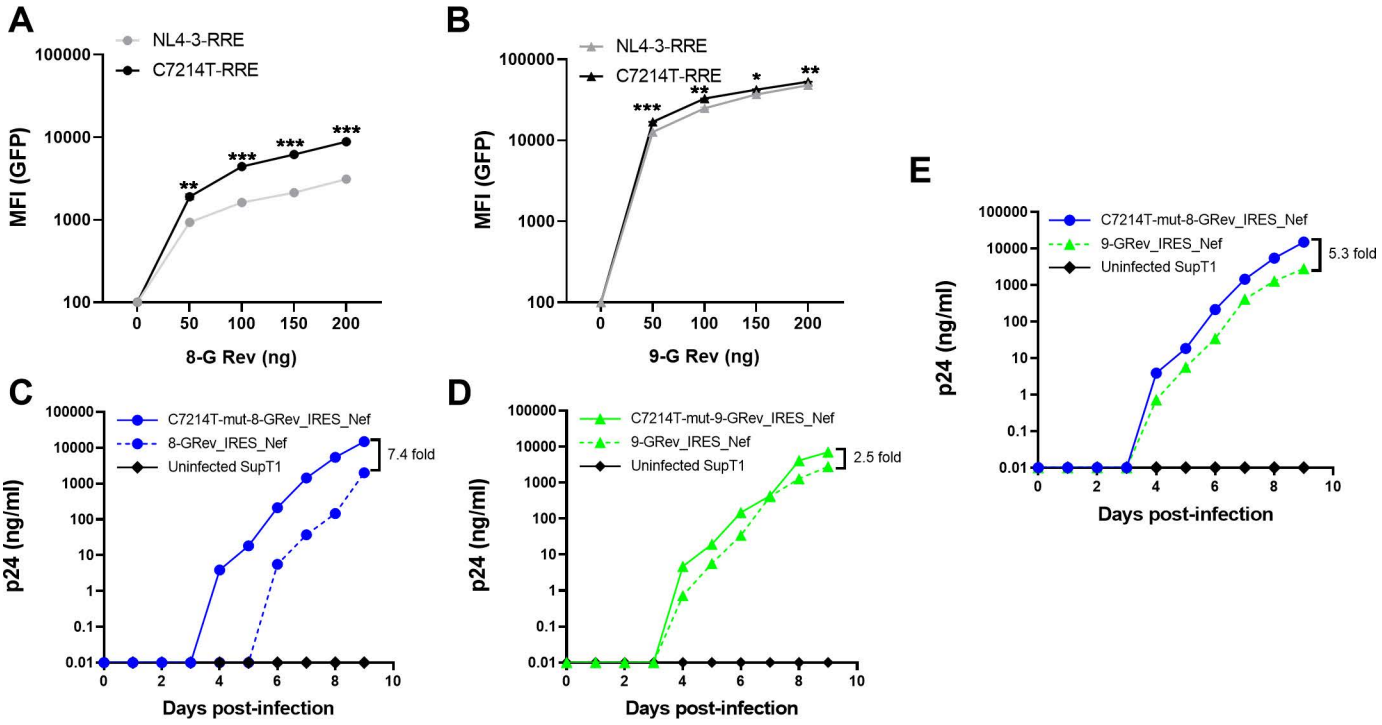

Fig 4. The C7214T mutation in the RRE enhances Rev-RRE dependent viral gene expression and viral replication. (A) 293T cells were co-transfected with a GFP reporter construct containing either the wild-type NL4-3 RRE or the C7214T mutant RRE, along with varying amounts of 8-G Rev expression plasmid. GFP mean fluorescence intensity (MFI) was measured by flow cytometry. **(B)** The Rev-RRE functional assay was performed as in (A) using 9-G Rev. **(C)** SupT1 cells were infected with 8-GRev_IRES_Nef and C7214T-mut8-GRev_IRES_Nef viruses at equal MOIs. Viral replication was monitored by p24 ELISA of culture supernatants over time. **(D)** Replication kinetics of 9-GRev_IRES_Nef and C7214T-mut9-GRev_IRES_Nef viruses were performed as in **(C)**. **(E)** Comparison of replication kinetics between C7214T-mut8-GRev and 9-GRev_IRES_Nef viruses. SupT1 cells were infected with equal MOIs of each virus. Viral replication was monitored by p24 ELISA of culture supernatants over time. Error bars in panels A and B represent mean ± SD from three independent experiments. Statistical analysis was performed using unpaired, two-tailed t-test with FDR correction for multiple comparisons (**$p < 0.01$, ***$p < 0.001$, ****$p < 0.0001$).

https://doi.org/10.1371/journal.ppat.1012885.g004

To assess the effect of Rev-RRE activity differences on reactivation from latency without the compounding effects of reinfection, resting primary CD4 + T cells were again latently infected with 8-GRev_IRES_Nef or 9-GRev_IRES_Nef viruses. Three days post-infection, cells were treated with LRAs or DMSO, and zidovudine (AZT), a nucleoside reverse transcriptase inhibitor, was added to prevent reinfection (Fig 5E). Supernatants and cells were collected through day 5 post-activation for analysis.

Following LRA treatment, it was observed that cells infected with the high Rev-RRE activity virus (9-GRev_IRES_Nef) released significantly more virus into the supernatant compared to the low Rev-RRE activity virus (8-GRev_IRES_Nef) (Fig 5F). Although the 8-GRev_IRES_Nef virus-infected cells exhibited some viral production post-activation, the levels were low and release was slow. Infected cells treated with DMSO alone did not reactivate as shown by only a background qRT-PCR signal.

To confirm that the difference in viral RNA production was not due to differences in cell viability, cell viability was measured in all conditions using trypan blue staining from day 1–5 post-reactivation (S5 Fig). This analysis showed no significant difference in cell viability between 8-GRev_IRES_Nef and 9-GRev_IRES_Nef infected cells (S5 Fig). Taken together, these experiments demonstrated that while differences in Rev/RRE activity does not affect the development of latency, high Rev/RRE activity significantly enhances viral reemergence and production once latently infected cells are reactivated.

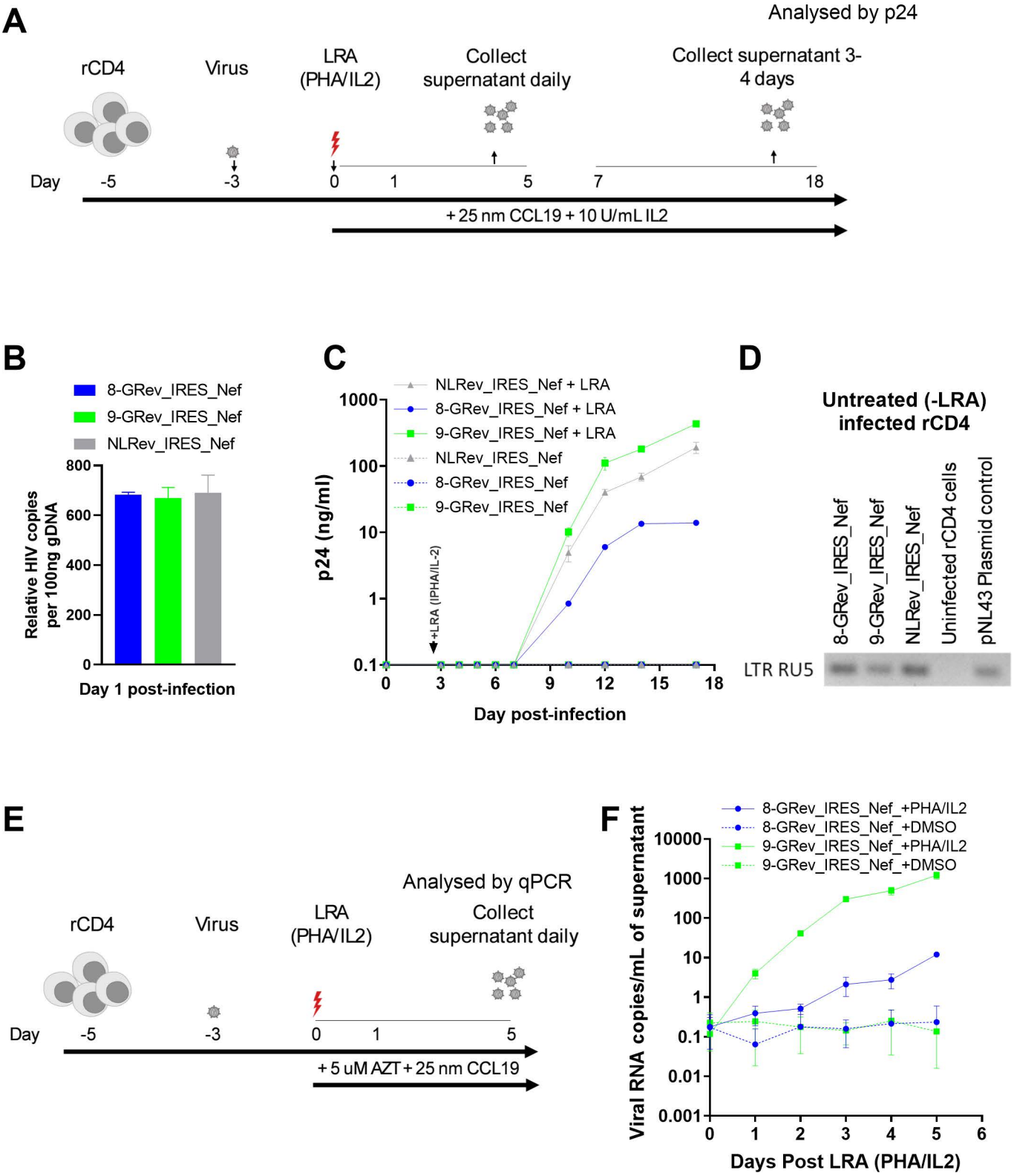

Fig 5. The high Rev-RRE activity viruses exhibits enhanced reactivation from latency and increased viral release compared to low Rev-RRE activity virus. (A) Schematic of the latency model and reactivation experiment. Resting primary CD4 + T cells were infected with 8-GRev_IRES_Nef, 9-GRev_IRES_Nef, or NLRev_IRES_Nef viruses. On day 3 post-infection, cells were treated with latency reversing agents (LRA: PHA + IL-2) or left

untreated. Culture supernatants were collected through day 17 post-infection. **(B)** Quantification of integrated provirus in infected resting CD4 + T cells 24 hours post-infection, measured by Alu-gag PCR. **(C)** Viral reactivation kinetics following LRA treatment. P24 levels in culture supernatants were measured by ELISA over time. Plotted p24 values represent corrected concentrations that account for the residual 50 μL of supernatant left behind after each media change. **(D)** Confirmation of integrated provirus in non-reactivated cells. A gel-based Alu-LTR PCR followed by LTR-RU5 amplification was used to qualitatively confirm the presence of integrated HIV-1 in cells that did not receive LRA at day 17 post-infection. This semi-quantitative assay indicates that cells remained latently infected without reactivation. **(E)** Schematic of the reactivation experiment without reinfection. Resting CD4 + T cells were infected with 8-GRev_IRES_Nef or 9-GRev_IRES_Nef viruses, treated with LRA or vehicle at day 3, and AZT was added to prevent reinfection. **(F)** Viral RNA copies/mL were measured by qRT-PCR using a standard curve derived from known amounts of NL4-3 RNA. Data represents mean ± SD from three independent experiments for panel B, mean ± SD from two independent experiments for panel C, and panel **F.** A and E were created in BioRender (Dzhivhuho, **G.**, 2025; https://BioRender.com/ak85scu).

https://doi.org/10.1371/journal.ppat.1012885.g005

Discussion

Using a reporter assay, in previous work, we showed significant variation in Rev-RRE activity among Rev proteins and RREs from primary HIV-1 isolates [23]. In this study, we now show that variation in Rev-RRE functional activity has significant impact on both viral replication kinetics and reactivation from latency. To analyze this, we engineered viruses with two Rev-RRE combinations that differed greatly in activity. We found that higher Rev-RRE activity confers an advantage in viral replication and that the high Rev-RRE activity virus outcompetes the low activity virus in co-infections. We also showed that high Rev-RRE activity leads to more efficient reactivation from latency in primary CD4 + T cells. The study provides proof of concept that Rev/RRE activity variation is an important modulator of these processes.

Interestingly, a spontaneous compensatory mutation in the RRE of the low Rev activity virus (8-GRev_IRES_Nef) was selected during passaging. This single nucleotide change in the RRE, within the initial Rev binding region, was sufficient to rescue the replication defect of the low-activity Rev virus and make its replication kinetics comparable to the high-activity Rev virus. This provides further support for the hypothesis that viruses with high Rev-RRE activity have a replication advantage when HIV is passaged *in vitro*. This is in stark contrast to the *in vivo* situation, where previous studies indicate that viruses with many varying levels of Rev-RRE activity are selected [23].

In previous work, we also analyzed Rev-RRE evolution *in vivo* [15]. In individuals living with HIV, but not on antiretroviral therapy, we observed a trend towards higher Rev-RRE activity in circulating viral variants over time, driven by changes in the RRE. In one individual, the accumulation of five nucleotide changes in the RRE over several years correlated with altered RRE secondary structure as well as increased functional activity [16]. The current study provides further evidence for the rapid selection of such mutations under conditions where Rev activity is limiting, emphasizing the biological significance of small RRE sequence changes.

Since the RRE also overlaps the envelope protein coding region, the C7214T mutation also led to an alanine to valine change in gp41, immediately adjacent to the start of the heptad repeat 1 (HR1) region. This mutation created an RRE with increased activity in our reporter assay, especially when tested with the 8-G Rev protein. This finding, combined with the fact that the mutation was only selected in the 8-GRev virus, strongly suggests that it was selected because it enhanced Rev-RRE function and not because it affected gp41 activity.

An in silico analysis (see S6 Fig) shows that T at position 7214 is particularly frequent in subtype G sequences, whereas subtypes A, B, C, CRF_AE, and CRF_AG predominantly harbor C at this locus (see Materials and Methods). The enrichment of T in subtype G is consistent with our findings that 8-G and 9-G Rev function best when 7214T is present, reinforcing a subtype G–specific adaptation in the HIV-1 RRE. Further studies, including structural probing or phylogenetic analyses, could clarify how multiple co-evolving mutations shape Rev-RRE compatibility in different viral subtypes.

Despite differences in replication kinetics, we observed that Nef expression levels were maintained at similar levels in both the high and low Rev activity virus. Nef enhances virion infectivity and is critical to maintaining high-titer replication *in vivo* [36]. Nef is a potent modulator of multiple cell surface molecules, including MHC-I, CD4, CD28, CCR5, SERINC3, and SERINC5. Nef also binds p53, suppressing its pro-apoptotic activity and potentially contributing to the survival of

infected cells [32,33,37–40]. By modulating the ratio of Nef expression to the expression of antigenic structural proteins like Gag and Env, viruses with low Rev activity are relatively protected from cytotoxic T cell-mediated killing *in vitro* [28]. A specific fitness landscape could thus lead to *in vivo* selection of optimal Rev-RRE activities to achieve a balance between immune evasion, cell survival, and replication capacity.

Our experiments also showed that Rev-RRE activity levels played a significant role in viral reactivation from latency. Cells infected with the high Rev-RRE activity virus produced virus more rapidly, and at higher levels, following activation with a latency-reversing agent, compared to cells infected with the low Rev-RRE activity virus. This was observed under conditions where activation led to a spreading infection, as well as when re-infection was blocked with a reverse transcriptase inhibitor, resulting in only first-round virus production.

HIV latent virus remains the primary barrier to a cure [41]. Latency reversing agents designed to overcome transcriptional blocks alone have proven inadequate in fully reversing latency [42–46], and post-transcriptional regulation of gene expression may be an additional important factor [47]. In this study we used PHA/IL-2 stimulation as a model for latency reversal, because it is one of the strongest transcriptional activators. Since Rev works at the post-transcriptional level, similar results would likely be seen with other transcriptional activators. The observation that differences in Rev-RRE functional activity alter the dynamics of reactivation adds a new layer of complexity to our understanding of persistence and may serve to advance cure strategies. Our studies suggest that effective latency reversal strategies may need to consider not only transcriptional activation, but also post-transcriptional regulation mediated by the Rev-RRE axis.

The ability to significantly alter viral replication kinetics through minimal sequence changes in either Rev or the RRE provides HIV with a flexible mechanism to optimize fitness in various environments. This plasticity may allow the virus to fine-tune replication in response to selective pressures encountered during infection, such as those encountered during transmission, in different body compartments, over the course of treated or untreated HIV infection, and in entry into and emergence from latency.

Conclusion

The results of our studies provide new insights into the complex relationship between Rev-RRE sequence variation, functional activity, and viral fitness. By demonstrating the impact of Rev-RRE activity on both replication kinetics and latency reactivation, we contribute to further understanding of how this regulatory axis affects HIV pathogenesis and persistence. These findings demonstrate the importance of post-transcriptional RNA regulation, both for HIV replication and latency, and demonstrate the importance of Rev-RRE functional variation in these processes.

Materials and methods

Cell Culture and Primary Cell Isolation

Cell Lines. HEK 293T/17 cells were cultured in Iscove's Modified Dulbecco's Medium (IMDM; Gibco) supplemented with 10% bovine calf serum (BCS; Cytiva) and 0.1% gentamicin (Gibco). SupT1 cells were maintained in RPMI 1640 medium with GlutaMAX (Gibco) supplemented with 10% fetal bovine serum (FBS; Cytiva) and 0.1% gentamicin. All cell lines were cultured at 37°C in a humidified incubator with 5% CO2.

Primary Cell Isolation and Culture. Resting CD4 + T cells were isolated from healthy donor buffy coats (American Red Cross) using the RosetteSep human CD4 + T cell enrichment cocktail (STEMCELL Technologies) according to manufacturer's protocol. Isolated cells were maintained in RPMI 1640 medium with GlutaMAX supplemented with 10% FBS, 0.1% gentamicin, and 10 IU/ml of human interleukin-2 (hIL-2) (Boehringer Mannheim) at 37°C with 5% CO2. For latency experiments, cells were cultured with 25 nM CCL19 (R&D Systems) for 2–3 days prior to infection. To confirm that CCL19-treated CD4 + T cells maintained a resting phenotype before infection, we stained an aliquot of cells with anti-CD69 (FITC) and anti-CD25 (PE) antibodies (see "Flow Cytometry" below) and analyzed them alongside a parallel aliquot that was stimulated for 24 hours with phytohemagglutinin (PHA) plus interleukin-2 (IL-2). Cells were gated on viable

CD4 + singlets, and CD69/CD25 expression was quantified by flow cytometry. Further details of the staining and gating strategy are provided in supporting information (S4 Fig).

Molecular Biology and Plasmid Construction

HIV-1 Molecular Clones. The HIV-1 molecular clones used in this study were derived from the pNL4–3 plasmid [48]. To facilitate manipulation of the Rev gene, which normally overlaps with both Env and Tat coding regions, we relocated Rev to an independent expression cassette. First, the native rev gene in pNL4–3 was functionally silenced through two modifications: the start codon was mutated from AUG to ACG, and a stop codon (UAA) was introduced at position 23 by mutating the original UAU codon. While this modification resulted in a serine to threonine substitution at amino acid position 70 in the overlapping Tat reading frame, functional assays confirmed that Tat activity was not impaired.

To enable Rev expression from an alternative location, we constructed an expression cassette containing a cDNA copy of the NL4–3 Rev gene followed by an internal ribosomal entry site (IRES). This cassette was inserted upstream of the Nef coding region, allowing both Rev and Nef to be expressed from what typically serves as the fully spliced mRNA encoding only Nef. To facilitate future modifications, the Rev sequence was flanked by unique restriction enzyme sites (*BamHI* downstream of Env and *MluI* upstream of the IRES).

Using this modified backbone, we generated two additional constructs incorporating Rev variants with different functional activities. The Rev sequences were obtained from previously characterized HIV-1 isolates: variant 8-G (GenBank accession FJ389367) and variant 9-G (GenBank accession JX140676), which exhibit approximately 4–5 fold difference in Rev activity when tested with the NL4–3 RRE [35]. These Rev variants were cloned into the modified backbone using the engineered restriction sites. The resulting proviral clones were designated pNLRev_IRES_Nef (HamRek archive #5833), p8-GRev_IRES_Nef (HamRek archive #5830), and p9-GRev_IRES_Nef (HamRek archive #5831).

Fluorescence-Based Reporter System. The fluorescence-based Rev-RRE functional assay system has been previously described in detail [23,35]. The system consists of two packageable viral constructs. The Rev expression vector was derived from pMSCV-IRES-Blue FP (Addgene plasmid #52115, gift from Dario Vignali), where Rev variants (8-G, 9-G, or NL4–3) were inserted upstream of the IRES and eBFP2 fluorescent marker. The RRE-containing reporter construct (HamRek archive #HR5604) contains a CHYSEL (2A-like peptide)-GFP (eGFP) cassette in the gag reading frame, an mCherry gene in place of Nef, and multiple modifications to ensure replication incompetence, including deletion of the gag myristoylation site, deletion of the gag-pol frameshift, two mutations in the first exon of Rev, and a frameshift mutation in Env.

C7214T RRE Mutation Construction. An RRE sequence containing a C7214T mutation, flanked by *BsaI* and *AleI* restriction sites, was synthesized by IDT. This modified RRE sequence was cloned into two existing vectors: 8-GRev_IRES_Nef (HamRek archive #5830) and 9-GRev_IRES_Nef (HamRek archive #5831), generating C7214T-mut8-GRev_IRES_Nef (HamRek archive #6468) and C7214T-mut9-GRev_IRES_Nef (HamRek archive #6470), respectively. The C7214T mutation was also introduced into the fluorescence-based reporter construct (HamRek archive #5604). The RRE region in this construct is flanked by *XmaI* and *XbaI* restriction sites. This facilitated the introduction of the modified sequence containing the C7214T mutation. This created the plasmid pHR6144 which was verified by DNA sequencing.

Bacterial Propagation and DNA Preparation. All molecular clones were propagated in NEB Stable Competent *E. coli* at 30°C in LB media supplemented with 50 μg/mL *Ampicillin*. Plasmid DNA was isolated using the ZymoPURE II Plasmid Maxiprep Kit (NEB), quantified by spectrophotometry (260/280 > 1.8), and verified by both restriction digest analysis and DNA sequencing across all modified regions.

Virus Production and Characterization

Initial Virus Production and Expansion. Initial viral stocks were generated by transfecting 293T cells with pNLRev_IRES_Nef (HamRek #5833), p8-GRev_IRES_Nef (HamRek #5830), or p9-GRev_IRES_Nef (HamRek #5831) plasmids.

After 48 hours, supernatants were collected and p24 levels were quantified by ELISA. For viral expansion, SupT1 cells (5×10^6 cells/ml) were infected with 100 ng p24 from the transfection supernatants in serum-free RPMI. DEAE-dextran was added to a final concentration of 8 μg/mL, and infection was facilitated by centrifugation at 380 RCF for one hour at 25°C. Following centrifugation, cells were washed with PBS and resuspended in RPMI supplemented with 10% FBS and gentamicin in 25 cm^2 flasks. Cultures were maintained by removing half of the cells and medium every 2–3 days, with the culture volume replenished with fresh medium.

Large-scale viral stocks were generated by infecting 15×10^6 SupT1 cells with 300 ng p24 from the peak viral expansion supernatant using the same infection protocol. Culture supernatants were collected every 4 days through day 16 post-infection, cleared of cells by centrifugation, and stored at -80°C. Viral replication was monitored by p24 ELISA, and stocks were titered by TCID50 assay. The day 8 stock, showing highest titer, was selected and used for subsequent experiments at an MOI of 0.005 for SupT1 cells and 0.05 for primary resting CD4 + T cells.

Replication Assays in Primary CD4⁺T Cells. Prior to infection, resting CD4⁺T cells were activated for 48 hours with 10 μg/mL PHA and 10 IU/mL IL-2. Cells were then infected at an MOI of 0.05 using spinoculation (1 hour, 25°C, 300 × g) to enhance viral entry, washed three times with room temperature 1X DPBS, and resuspended in RPMI supplemented with 10% FBS and 10 IU/mL IL-2 so that each well in a 96-well plate received 1×10^6 cells in a final volume of 250 μL. Every 3–4 days, 200 μL of supernatant was collected and replaced with fresh 200 μL of media. p24 was measured by ELISA, and the plotted values represent corrected concentrations that account for the residual 50 μL of supernatant left behind after each media change, ensuring an accurate representation of cumulative viral replication over time. The correction is applied using the following formula: Corrected p24 = Measured p24 + (Previous p24 × 0.2). Here, 0.2 corresponds to the residual fraction of 50 μL in 250 μL.

Analytical Methods

CD4 Downmodulation Assay. Following infection of SupT1 cells with viral constructs (8-GRev_IRES_Nef, 9-GRev_IRES_Nef, or NLRev_IRES_Nef) at an MOI of 0.005 for 8 days, cells were harvested and washed with 1X DPBS. Cells were blocked with human serablock (Bio-Rad) and stained with Mouse-anti hCD4-PE conjugated antibody (R&D Systems) for 30 minutes at 4°C. After two washes, cells were fixed with 4% formaldehyde-PBS for 10 minutes and permeabilized with 0.5% triton X-100 for 10 minutes. Intracellular p24 was detected using anti-HIV-p24-FITC conjugated antibody (NIH HIV Reagent Program) for 1 hour at 4°C protected from light. Cells infected with a Nef-negative NL4–3 virus derived from the plasmid HamRek #1272 served as a control.

Confirmation of Resting Phenotype. Following thawing and an initial 2–3-day incubation with 25 nM CCL19, an aliquot of CD4 + T cells was treated with phytohemagglutinin (PHA; 10 μg/mL) and 10 IU/mL IL-2 for 24 hours under standard culture conditions, while a parallel aliquot remained in media alone. At 24 hours post-treatment, cells were washed once in cold PBS and blocked with 2% bovine serum albumin (BSA) in PBS for 20 minutes at 4°C to reduce nonspecific binding. A 1 × Live/Dead viability stain (ThermoFisher) was then applied for 20 minutes at 4°C, followed by staining with anti-CD4 (AF700), anti-CD25 (PE), and anti-CD69 (FITC) antibodies (all from Cell Signaling, at a 1:100 dilution) for an additional 45 minutes at 4°C in the dark. After three washes with PBS, samples were analyzed on an Attune NxT flow cytometer (ThermoFisher Scientific), acquiring at least 50,000 singlet events per condition.

Rev-RRE Functional Activity Analysis. Rev-RRE functional activity was assessed through co-transfection experiments in 293T cells. Cells were seeded at 2×10^5 cells per well in 12-well plates in IMDM with 10% BCS. After 24 hours, media was replaced with serum-free IMDM, and cells were co-transfected using PEI with 1 μg of RRE-containing GFP reporter construct (either wild-type NL4–3 RRE or C7214T mutant RRE) and varying amounts of Rev expression plasmid (0, 50, 100, 150, or 200 ng of 8-G or 9-G Rev variants). Six hours post-transfection, media was replaced with IMDM containing 10% BCS. Cells were incubated at 37°C in 5% CO_2 for 48 hours.

At 48 hours post-transfection, 293T cells were trypsinized and washed twice with cold PBS. Cells were analyzed by flow cytometry using a sequential gating strategy. First, forward and side scatter was used to identify viable cells. This was followed by single-cell discrimination, and selection of the mCherry and BFP double-positive population. To assess Rev-RRE functional activity, GFP mean fluorescence intensity (MFI) was determined in this double-positive population using FlowJo software.

All flow cytometry was performed using an Attune NxT with autosampler (Thermo Fischer Scientific). Single-color controls were used for compensation calculations in FlowJo software (v10.6.1, BD Biosciences).

PCR and Sequencing

DNA Extraction. Cells were washed twice with cold PBS, and genomic DNA was extracted using the DNeasy Blood & Tissue Kit (Qiagen) following manufacturer's instructions.

Alu-gag PCR for Proviral Detection. Integrated provirus was detected using a nested PCR approach. First-round PCR used 150 ng genomic DNA with forward Alu primer (5'-GCC TCC CAA AGT GCT GGG ATT ACA G-3') and reverse HIV Gag primer (5'-GTT CCT GCT ATG TCA CTT CC-3'). PCR conditions were initial denaturation at 95°C for 2 minutes; followed by 25 cycles of 95°C for 15 seconds, 50°C for 30 seconds, and 72°C for 4 minutes 30 seconds. Second-round PCR used 2 µL of first-round product with forward LTR-R primer (5'-TTA AGC CTC AAT AAA GCT TGC C-3') and reverse U5 primer (5'-GTT CGG GCG CCA CTG CTA GA-3'). Second-round conditions were initial denaturation at 95°C for 2 minutes, followed by 35 cycles of 95°C for 15 seconds, 50°C for 30 seconds, and 72°C for 30 seconds. PCR products were visualized by electrophoresis for the ~100 bp RU5 product.

Competition Assay. SupT1 cells were co-infected in triplicate with 8-GRev_IRES_Nef and 9-GRev_IRES_Nef viruses at an MOI of 0.005 each. Cellular DNA was collected on days 1, 3, 5, and 7 post-infection. The relative proportion of integrated viruses was determined by discriminative PCR using 200 ng genomic DNA template in 50 µL reactions containing Taq DNA polymerase (Thermo Scientific), 2 pmol env forward primer (5'-CCTAGAAGAATAAGACAGGGC-3'), and 1 pmol each of variant-specific reverse primers: 8-G-specific (5'-CCCCAGATATTTCAGGCCCTC-3') and 9-G-specific (5'-GTCTCTCAAGCGGTGGTAGCAC-3'). PCR cycling conditions were initial denaturation at 95°C for 3 minutes; 25 cycles of 94°C for 30 seconds, 60°C for 30 seconds, and 75°C for 45 seconds; followed by final extension at 72°C for 10 minutes.

PCR products (15 µL) were separated on 2% ultrapure agarose gels (Invitrogen) containing ethidium bromide at 80V for 2 hours. Gels were imaged using a Bio-Rad transilluminator with optimized exposure settings to prevent band saturation. Band intensities were quantified using Image Lab software (Bio-Rad). Standard curves were generated using known ratios of 8-GRev and 9-GRev plasmids, which were also amplified separately or together as PCR controls. The relative proportion of each variant was expressed as a percentage of total signal from both PCR bands per lane.

RRE and Rev Sequencing Analysis. To analyze potential mutations, both RRE and Rev regions of proviruses were amplified using nested PCR. First-round PCR reactions contained 150 ng genomic DNA template in 25 µL reactions containing: 1X PCR buffer, 1.8 mM MgSO4, 0.2 mM each dNTP, 0.2 µM each primer, and 1 U high-fidelity Taq DNA Polymerase (Invitrogen). For RRE amplification, first-round primers were 5'-GTGACACAATCACACTCCCATGC-3' (forward) and 5'-GGTGAATATCCCTGCCTAACTC-3' (reverse), followed by second-round primers 5'-CAATGGGTCCGAGATCTTCAGACC-3' (forward) and 5'-CACTCCATCCAGGTCATGTTATTC-3' (reverse). Rev amplification used first-round primers 5'-GCACTTATCTGGGACGATCTGCG-3' (forward) and 5'-GCTTCCTTCACGACATTCAACAG-3' (reverse), followed by second-round primers 5'-CCTACAGTATTGGAGTCAGGAAC-3' (forward) and 5'-GGAATGCTCGTCAAGAAGACAGGGCC-3' (reverse).

PCR conditions for both rounds consisted of initial denaturation at 94°C for 3 minutes, followed by 20 cycles of denaturation at 94°C for 30 seconds, annealing at 52°C (first round) or 53°C (second round) for 30 seconds, and extension at 68°C for 50 seconds, with a final extension at 68°C for 10 minutes. Second-round PCR used 5 µL of first-round product

as template. PCR products were visualized on 2% agarose gels containing ethidium bromide, extracted and subjected to Sanger sequencing. All reactions were performed in duplicate to ensure reproducibility.

Bioinformatic Analysis of RRE Sequences. Publicly available HIV-1 RRE sequences (subtypes A, B, C, G, CRF_AE, CRF_AG) were downloaded from the Los Alamos HIV Database (https://www.hiv.lanl.gov/) on [date accessed October 20, 2024]. Sequences were aligned to the NL4–3 reference genome (GenBank U26942) using Geneious Prime 2 (v2022.2.2). We extracted the nucleotide present at position 7214 in each sequence to determine the proportion of sequences harboring C versus T.

Protein Analysis

Western Blot Analysis. Infected cells were harvested and washed twice with 1X Dulbecco's Phosphate-Buffered Saline (DPBS; Invitrogen). Cell pellets were lysed in buffer containing 1 mM sodium chloride, 1X protease inhibitor cocktail, 1 mM EDTA (pH 7.4), and 1% SDS by heating at 95°C for 10 minutes. Lysates were cleared by centrifugation (14,000 × g, 10 minutes, room temperature), and supernatants were mixed 1:1 with LDS Sample Buffer (Invitrogen) and heated at 72°C for 10 minutes. Equal volumes of protein lysate were separated on NuPAGE 4–12% Bis-Tris (MES) gels (Invitrogen) under reducing conditions and transferred to PVDF membranes using the Trans-Blot Turbo Transfer System (Bio-Rad) at 30V for 1 hour.

Membranes were blocked with iBind Flex Solution (Thermo Fisher Scientific) for 10 minutes at room temperature. Primary antibodies (mouse anti-p24 and mouse anti-Nef monoclonal antibodies (NIH HIV Reagent Program, Division of AIDS, NIAID, NIH), both at 1:1000 dilution and secondary antibody (IRDye 800CW Goat anti-Mouse IgG, LI-COR Biosciences, 1:6000 dilution) were applied using an iBind Flex Western System (Thermo Fisher Scientific) for 2.5 hours at room temperature. Beta-tubulin served as loading control for normalization. Protein bands were visualized using an Odyssey CLx chemifluorescence detector (LI-COR Biosciences) and quantified using ImageStudio software version 5.2 (LI-COR Biosciences). All western blot analyses were performed with at least three biological replicates.

Latency Model Experiments

Establishment of Latent Infection. Latent infection was established using a modified version of the Lewin model. Following CCL19 treatment (described in section 1.2), latent infection was initiated by spinoculation of 2×10^6 cells with HIV-1 Rev-variant molecular clones at an MOI of 0.05 for 2 hours at 300 × g at room temperature. Following spinoculation, cells were washed three times with room temperature 1X DPBS to remove residual virus and maintained in culture media supplemented with 25 nM CCL19 and 10 IU/ml IL-2.

Latency Reversal Analysis. Three days post-infection, latently infected cells were divided for two parallel reactivation experiments. In the first approach, cells were reactivated using 10 μg/mL phytohemagglutinin (PHA) (Sigma-Aldrich) and 10 IU/mL IL-2. Virus outgrowth was monitored for up to 17 days by p24 ELISA of culture supernatants. In the second approach, reactivation was performed in the presence of 5 nM zidovudine (AZT) (NIH HIV Reagent Program) to prevent reinfection, and virus production was monitored for 5 days post-reactivation.

Viral RNA Analysis and Quantification. Supernatants from AZT-treated cultures were collected daily and processed for RNA analysis. Samples were cleared of cellular debris by centrifugation (5300 RCF, 5 minutes, 4°C), and viruses were pelleted by centrifugation at 16,000 RCF for 1 hour at 4°C. Virus pellets were resuspended in 50 μL RNase-free 5 mM Tris-HCL (pH 8.0) and treated with 10 μL proteinase K (20 mg/mL) at 55°C for 30 minutes. RNA was isolated by adding 200 μL of 6 M guanidinium isothiocyanate and 10 μL glycogen (20 mg/mL), followed by isopropanol precipitation. RNA pellets were washed with 70% ethanol and resuspended in 40 μL RNase-free Tris-HCL. cDNA synthesis was performed using the SuperScript IV Reverse Transcriptase kit with oligo(dT)20 primer.

Viral RNA was quantified by qPCR using 2 μL cDNA template with the Luna TaqMan Master Mix (NEB) on an ABI Step One Plus thermocycler. Reactions contained 0.3 nM each primer (LTR-R forward: 5'-TTA AGC CTC AAT AAA GCT TGC

C-3'; U5 reverse: 5'-GTT CGG GCG CCA CTG CTA GA-3') and 0.2 nM of double quenched RU5-specific probe (5'-/56-FAM/CCAGAGTCA/ZEN/CACAACAGACGGGCACA/3IABkFQ/-3'). PCR conditions were initial denaturation at 95°C for 1 minute, followed by 40 cycles of 95°C for 15 seconds and 60°C for 30 seconds. Standard curves were generated using 10-fold serial dilutions of predetermined NL4–3 cDNA from TCID50-quantified virus, with values converted to infectious units per mL supernatant. Results were analyzed using StepOne Software v2.3. To ensure RNA specificity and exclude DNA contamination, control reactions were performed on supernatant samples without reverse transcriptase treatment. These controls confirmed the absence of contaminating HIV DNA in the supernatant nucleic acid preparations.

Cell Viability. Cell viability was assessed using the Trypan Blue exclusion method. Cells were mixed with an equal volume of 0.4% Trypan Blue solution (Gibco) and counted using a hemocytometer.

Statistical Analysis

Statistical analyses were performed using GraphPad Prism software version 8.0.1 (GraphPad Software, USA). For experiments with three independent replicates, statistical comparisons were conducted using unpaired, two-tailed t-tests, with false discovery rate (FDR) correction applied for multiple comparisons. P-values < 0.05 were considered statistically significant. For experiments with two independent replicates, only descriptive statistics were calculated. All data are presented as mean ± standard deviation (SD) or standard error of the mean (SEM) as indicated in figure legends.

Supporting information

S1 Fig. Generation and characterization of viral stocks from modified HIV proviral clones. (A) Schematic representation of the virus propagation strategy. (B) 293T cells were transfected with pNLRev_IRES_Nef (HamRek #5833), p8-GRev_IRES_Nef (HamRek #5830), p9-GRev-IRES_Nef (HamRek #5831), and original pNL4–3 plasmids. P24 levels in supernatants were measured 48 hours post-transfection. (C) Initial infection kinetics in SupT1 cells ($1x10^6$ cells/ml) using 100 ng p24 from transfection supernatants. Peak viremia timepoints were selected for large stock production. (D) Infection kinetics in SupT1 cells using peak p24 virus stock from (C) to generate final expanded viral stocks. TCID50 was determined for these stocks. Day 8 stock, which showed the highest titer, was used for infection in subsequent experiments.
(TIF)

S2 Fig. Comparison of replication kinetics in primary CD4⁺T cells. Resting CD4⁺T cells were pre-activated for 48 hours with PHA (10 μg/mL) plus IL-2 (10 IU/mL) and then infected at an MOI of 0.05 by spinoculation for 1 hour at room temperature. Cells were washed three times with room temperature 1X DPBS to remove unbound virus, cultured in RPMI supplemented with 10% FBS and IL-2, and supernatants were collected every 3–4 days for p24 quantification. Plotted p24 values represent corrected concentrations that account for the residual 50 μL of supernatant left behind after each media change. The 9-GRev_IRES_Nef virus (green) consistently replicated more efficiently than 8-GRev_IRES_Nef (blue), consistent with observations in SupT1 cells. Data are mean ± SEM from triplicate experiments.
(TIF)

S3 Fig Confirmation of Rev cassette integrity and stability over time. Late-timepoint (day 10) infected SupT1 cells were harvested, and total genomic DNA was subjected to PCR and Sanger sequencing. The sequencing chromatograms show that neither the introduced stop codon (UAA, replacing the native UAU) nor the disrupted start codon (ACG, replacing AUG) in exon 1 of rev underwent reversion during viral replication. These findings confirm that the relocated Rev-IRES-Nef cassette remained intact and that no selective advantage for revertants was observed under our experimental conditions.
(TIF)

S4 Fig. Phenotypic characterization of resting versus activated primary CD4+T cells by flow cytometry. (A) The Gating strategy used to identify live CD4+T cells from total events: live cells were first selected, followed by gating on $CD4^+$ singlets. (B) Representative dot plot showing minimal CD69 and CD25 expression in CCL19-treated, resting CD4+T cells. (C) Corresponding dot plot of activated $CD4^+$T cells treated with phytohaemagglutinin (PHA) plus interleukin-2 (IL-2) for 24 hours, demonstrating robust upregulation of both CD69 and CD25. (D) Histograms comparing CD69 expression levels in resting (blue) versus activated (red) cells. (E) Histograms comparing CD25 expression in resting (blue) versus activated (red) cells. Taken together, these data confirm that CCL19 maintains cells in a quiescent state, whereas PHA/IL-2 triggers a high-activation phenotype.
(TIF)

S5 Fig. Viability of resting CD4+T cells from the AZT-treated latency reactivation experiment. Cell viability of resting CD4+T cells latently infected with 8-GRev_IRES_Nef or 9-GRev_IRES_Nef viruses, treated with latency reversing agents (LRA) or DMSO vehicle at day 3 post-infection, and cultured in the presence of zidovudine (AZT) to prevent reinfection. Cell viability was assessed using trypan blue staining from day 1–5 post-reactivation. The graph shows the percentage of viable cells over time for both viral constructs under LRA and AZT treatment conditions.
(TIF)

S6 Fig. Frequency of the C7214T SNP within the HIV-1 RRE across major subtypes. To assess whether C7214T is commonly present in naturally circulating HIV-1 strains, we surveyed RRE sequences from multiple subtypes in the Los Alamos HIV Database, as described in Materials and Methods. Each pie chart depicts the proportion of sequences harboring thymidine (T) versus cytidine (C) at position 7214 (relative to NL4–3 numbering) among major HIV-1 subtypes: A (n = 96), B (n = 70,689), C (n = 29,733), G (n = 603), CRF_AE (n = 10,059), and CRF_AG (n = 1,242).
(TIF)

S1 Table. Numerical data for Fig 1.
(XLSX)

S2 Table. Numerical data for Fig 2.
(XLSX)

S3 Table. Numerical data for Fig 3.
(XLSX)

S4 Table. Numerical data for Fig 4.
(XLSX)

S5 Table. Numerical data for Fig 5.
(XLSX)

S6 Table. Numerical Data for All Supporting Figures.
(XLSX)

S1 File. Sequence files for S3 Fig. These files contain the Rev coding exon 1 sequences in the native position, and complete Rev sequences in the Rev-IRES Nef cassette, of the integrated proviruses from the virus infections as indicated.
(ZIP)

S2 File. Sequence files for Fig 3. These files contain RRE sequences of the integrated proviruses from the virus infections as indicated.
(ZIP)

Acknowledgments

Monoclonal antibodies were obtained through the NIH HIV Reagent Program, Division of AIDS, NIAID, NIH. The anti-HIV-1 Nef antibody (AE6, ARP-709) was contributed by Dr. James Hoxie and the monoclonal anti-HIV-1 p24 antibody (183-H12-5C, ARP-3537) was contributed by Dr. Bruce Chesebro and Kathy Wehrly.

Author contributions

Conceptualization: Marie-Louise Hammarskjold, David Rekosh.

Data curation: Godfrey A. Dzhivhuho.

Formal analysis: Godfrey A. Dzhivhuho, Patrick E.H. Jackson, Marie-Louise Hammarskjold, David Rekosh.

Funding acquisition: Patrick E.H. Jackson, Marie-Louise Hammarskjold, David Rekosh.

Investigation: Godfrey A. Dzhivhuho, Patrick E.H. Jackson, Ethan S. Honeycutt, Flavio da Silva Mesquita, Jing Huang.

Methodology: Godfrey A. Dzhivhuho, Patrick E.H. Jackson, Ethan S. Honeycutt, Flavio da Silva Mesquita, Jing Huang, Marie-Louise Hammarskjold, David Rekosh.

Project administration: Marie-Louise Hammarskjold, David Rekosh.

Resources: Marie-Louise Hammarskjold, David Rekosh.

Supervision: Godfrey A. Dzhivhuho, Marie-Louise Hammarskjold, David Rekosh.

Writing – original draft: Godfrey A. Dzhivhuho, Patrick E.H. Jackson.

Writing – review & editing: Godfrey A. Dzhivhuho, Patrick E.H. Jackson, Marie-Louise Hammarskjold, David Rekosh.

References

1. Bray M, Prasad S, Dubay JW, Hunter E, Jeang KT, Rekosh D, et al. A small element from the Mason-Pfizer monkey virus genome makes human immunodeficiency virus type 1 expression and replication Rev-independent. Proc Natl Acad Sci U S A. 1994;91(4):1256–60. https://doi.org/10.1073/pnas.91.4.1256 PMID: 8108397
2. Rekosh D, Hammarskjold ML. Intron retention in viruses and cellular genes: Detention, border controls and passports. Wiley Interdisciplinary Reviews RNA. 2018;9(3):e1470.
3. Hadzopoulou-Cladaras M, Felber BK, Cladaras C, Athanassopoulos A, Tse A, Pavlakis GN. The rev (trs/art) protein of human immunodeficiency virus type 1 affects viral mRNA and protein expression via a cis-acting sequence in the env region. J Virol. 1989;63(3):1265–74. https://doi.org/10.1128/JVI.63.3.1265-1274.1989 PMID: 2783738
4. Hammarskjöld ML, Heimer J, Hammarskjöld B, Sangwan I, Albert L, Rekosh D. Regulation of human immunodeficiency virus env expression by the rev gene product. J Virol. 1989;63(5):1959–66. https://doi.org/10.1128/JVI.63.5.1959-1966.1989 PMID: 2704072
5. Malim MH, Hauber J, Le SY, Maizel JV, Cullen BR. The HIV-1 rev trans-activator acts through a structured target sequence to activate nuclear export of unspliced viral mRNA. Nature. 1989;338(6212):254–7. https://doi.org/10.1038/338254a0 PMID: 2784194
6. Fernandes JD, Booth DS, Frankel AD. A structurally plastic ribonucleoprotein complex mediates post-transcriptional gene regulation in HIV-1. Wiley Interdiscip Rev RNA. 2016;7(4):470–86. https://doi.org/10.1002/wrna.1342 PMID: 26929078
7. Neville M, Stutz F, Lee L, Davis LI, Rosbash M. The importin-beta family member Crm1p bridges the interaction between Rev and the nuclear pore complex during nuclear export. Curr Biol. 1997;7(10):767–75. https://doi.org/10.1016/s0960-9822(06)00335-6 PMID: 9368759
8. Askjaer P, Jensen TH, Nilsson J, Englmeier L, Kjems J. The specificity of the CRM1-Rev nuclear export signal interaction is mediated by RanGTP. J Biol Chem. 1998;273(50):33414–22. https://doi.org/10.1074/jbc.273.50.33414 PMID: 9837918
9. Fornerod M, Ohno M, Yoshida M, Mattaj IW. CRM1 is an export receptor for leucine-rich nuclear export signals. Cell. 1997;90(6):1051–60. https://doi.org/10.1016/s0092-8674(00)80371-2 PMID: 9323133
10. Fukuda M, Asano S, Nakamura T, Adachi M, Yoshida M, Yanagida M, et al. CRM1 is responsible for intracellular transport mediated by the nuclear export signal. Nature. 1997;390(6657):308–11. https://doi.org/10.1038/36894 PMID: 9384386
11. Booth DS, Cheng Y, Frankel AD. The export receptor Crm1 forms a dimer to promote nuclear export of HIV RNA. eLife. 2014;3:e04121.
12. Watts JM, Dang KK, Gorelick RJ, Leonard CW, Bess JW Jr, Swanstrom R, et al. Architecture and secondary structure of an entire HIV-1 RNA genome. Nature. 2009;460(7256):711–6. https://doi.org/10.1038/nature08237 PMID: 19661910

13. Sherpa C, Rausch JW, Le Grice SFJ, Hammarskjold M-L, Rekosh D. The HIV-1 Rev response element (RRE) adopts alternative conformations that promote different rates of virus replication. Nucleic Acids Res. 2015;43(9):4676–86. https://doi.org/10.1093/nar/gkv313 PMID: 25855816
14. Daugherty MD, Liu B, Frankel AD. Structural basis for cooperative RNA binding and export complex assembly by HIV Rev. Nat Struct Mol Biol. 2010;17(11):1337–42. https://doi.org/10.1038/nsmb.1902 PMID: 20953181
15. Sloan EA, Kearney MF, Gray LR, Anastos K, Daar ES, Margolick J, et al. Limited nucleotide changes in the Rev response element (RRE) during HIV-1 infection alter overall Rev-RRE activity and Rev multimerization. J Virol. 2013;87(20):11173–86. https://doi.org/10.1128/JVI.01392-13 PMID: 23926352
16. Sherpa C, Jackson PEH, Gray LR, Anastos K, Le Grice SFJ, Hammarskjold M-L, et al. Evolution of the HIV-1 Rev Response Element during Natural Infection Reveals Nucleotide Changes That Correlate with Altered Structure and Increased Activity over Time. J Virol. 2019;93(11):e02102-18. https://doi.org/10.1128/JVI.02102-18 PMID: 30867301
17. Shuck-Lee D, Chang H, Sloan EA, Hammarskjold M-L, Rekosh D. Single-nucleotide changes in the HIV Rev-response element mediate resistance to compounds that inhibit Rev function. J Virol. 2011;85(8):3940–9. https://doi.org/10.1128/JVI.02683-10 PMID: 21289114
18. Hamm TE, Rekosh D, Hammarskjold ML. Selection and characterization of human immunodeficiency virus type 1 mutants that are resistant to inhibition by the transdominant negative RevM10 protein. J Virol. 1999;73(7):5741–7.
19. Jain C, Belasco JG. Structural model for the cooperative assembly of HIV-1 Rev multimers on the RRE as deduced from analysis of assembly-defective mutants. Mol Cell. 2001;7(3):603–14. https://doi.org/10.1016/s1097-2765(01)00207-6 PMID: 11463385
20. Fischer U, Huber J, Boelens WC, Mattaj IW, Luhrmann R. The HIV-1 Rev activation domain is a nuclear export signal that accesses an export pathway used by specific cellular RNAs. Cell. 1995;82(3):475–83.
21. Battiste JL, Mao H, Rao NS, Tan R, Muhandiram DR, Kay LE, et al. Alpha helix-RNA major groove recognition in an HIV-1 rev peptide-RRE RNA complex. Science. 1996;273(5281):1547–51. https://doi.org/10.1126/science.273.5281.1547 PMID: 8703216
22. Venkatesh LK, Mohammed S, Chinnadurai G. Functional domains of the HIV-1 rev gene required for trans-regulation and subcellular localization. Virology. 1990;176(1):39–47. https://doi.org/10.1016/0042-6822(90)90228-j PMID: 2109912
23. Jackson PE, Tebit DM, Rekosh D, Hammarskjold ML. Rev-RRE Functional Activity Differs Substantially Among Primary HIV-1 Isolates. AIDS research and human retroviruses. 2016;32(9):923–34.
24. Dzhivhuho G, Holsey J, Honeycutt E, O'Farrell H, Rekosh D, Hammarskjold M-L, et al. HIV-1 Rev-RRE functional activity in primary isolates is highly dependent on minimal context-dependent changes in Rev. Sci Rep. 2022;12(1):18416. https://doi.org/10.1038/s41598-022-21714-2 PMID: 36319640
25. Belshan M, Harris ME, Shoemaker AE, Hope TJ, Carpenter S. Biological characterization of Rev variation in equine infectious anemia virus. J Virol. 1998;72(5):4421–6. https://doi.org/10.1128/JVI.72.5.4421-4426.1998 PMID: 9557734
26. Belshan M, Baccam P, Oaks JL, Sponseller BA, Murphy SC, Cornette J, et al. Genetic and biological variation in equine infectious anemia virus Rev correlates with variable stages of clinical disease in an experimentally infected pony. Virology. 2001;279(1):185–200. https://doi.org/10.1006/viro.2000.0696 PMID: 11145901
27. Baccam P, Thompson RJ, Li Y, Sparks WO, Belshan M, Dorman KS, et al. Subpopulations of equine infectious anemia virus Rev coexist in vivo and differ in phenotype. J Virol. 2003;77(22):12122–31. https://doi.org/10.1128/jvi.77.22.12122-12131.2003 PMID: 14581549
28. Bobbitt KR, Addo MM, Altfeld M, Filzen T, Onafuwa AA, Walker BD, et al. Rev activity determines sensitivity of HIV-1-infected primary T cells to CTL killing. Immunity. 2003;18(2):289–99. https://doi.org/10.1016/s1074-7613(03)00031-1 PMID: 12594955
29. Phuphuakrat A, Paris RM, Nittayaphan S, Louisirirotchanakul S, Auewarakul P. Functional variation of HIV-1 Rev Response Element in a longitudinally studied cohort. J Med Virol. 2005;75(3):367–73. https://doi.org/10.1002/jmv.20279 PMID: 15648073
30. Phuphuakrat A, Auewarakul P. Functional variability of Rev response element in HIV-1 primary isolates. Virus Genes. 2005;30(1):23–9. https://doi.org/10.1007/s11262-004-4578-9 PMID: 15744559
31. Jackson PEH, Holsey J, Turse L, Hammarskjold M-L, Rekosh D. Rev–Rev Response Element Activity Selection Bias at the Human Immunodeficiency Virus Transmission Bottleneck. Open Forum Infectious Diseases. 2023;10(10).
32. Chaudhuri R, Lindwasser OW, Smith WJ, Hurley JH, Bonifacino JS. Downregulation of CD4 by human immunodeficiency virus type 1 Nef is dependent on clathrin and involves direct interaction of Nef with the AP2 clathrin adaptor. J Virol. 2007;81(8):3877–90. https://doi.org/10.1128/JVI.02725-06 PMID: 17267500
33. Greenberg ME, Bronson S, Lock M, Neumann M, Pavlakis GN, Skowronski J. Co-localization of HIV-1 Nef with the AP-2 adaptor protein complex correlates with Nef-induced CD4 down-regulation. EMBO J. 1997;16(23):6964–76. https://doi.org/10.1093/emboj/16.23.6964 PMID: 9384576
34. Jayaraman B, Crosby DC, Homer C, Ribeiro I, Mavor D, Frankel AD. RNA-directed remodeling of the HIV-1 protein Rev orchestrates assembly of the Rev-Rev response element complex. Elife. 2014;3:e04120. https://doi.org/10.7554/eLife.04120 PMID: 25486594
35. Jackson PEH, Huang J, Sharma M, Rasmussen SK, Hammarskjold M-L, Rekosh D. A novel retroviral vector system to analyze expression from mRNA with retained introns using fluorescent proteins and flow cytometry. Sci Rep. 2019;9(1):6467. https://doi.org/10.1038/s41598-019-42914-3 PMID: 31015546
36. Peterlin BM, Trono D. Hide, shield and strike back: how HIV-infected cells avoid immune eradication. Nat Rev Immunol. 2003;3(2):97–107. https://doi.org/10.1038/nri998 PMID: 12563294

37. Fackler OT, Baur AS. Live and let die: Nef functions beyond HIV replication. Immunity. 2002;16(4):493–7. https://doi.org/10.1016/s1074-7613(02)00307-2 PMID: 11970873

38. Michel N, Allespach I, Venzke S, Fackler OT, Keppler OT. The Nef protein of human immunodeficiency virus establishes superinfection immunity by a dual strategy to downregulate cell-surface CCR5 and CD4. Curr Biol. 2005;15(8):714–23. https://doi.org/10.1016/j.cub.2005.02.058 PMID: 15854903

39. Usami Y, Wu Y, Göttlinger HG. SERINC3 and SERINC5 restrict HIV-1 infectivity and are counteracted by Nef. Nature. 2015;526(7572):218–23. https://doi.org/10.1038/nature15400 PMID: 26416733

40. Rosa A, Chande A, Ziglio S, De Sanctis V, Bertorelli R, Goh SL, et al. HIV-1 Nef promotes infection by excluding SERINC5 from virion incorporation. Nature. 2015;526(7572):212–7. https://doi.org/10.1038/nature15399 PMID: 26416734

41. Richman DD, Margolis DM, Delaney M, Greene WC, Hazuda D, Pomerantz RJ. The challenge of finding a cure for HIV infection. Science. 2009;323(5919):1304–7. https://doi.org/10.1126/science.1165706 PMID: 19265012

42. Bullen CK, Laird GM, Durand CM, Siliciano JD, Siliciano RF. New ex vivo approaches distinguish effective and ineffective single agents for reversing HIV-1 latency in vivo. Nat Med. 2014;20(4):425–9. https://doi.org/10.1038/nm.3489 PMID: 24658076

43. Laird GM, Bullen CK, Rosenbloom DIS, Martin AR, Hill AL, Durand CM, et al. Ex vivo analysis identifies effective HIV-1 latency-reversing drug combinations. J Clin Invest. 2015;125(5):1901–12. https://doi.org/10.1172/JCI80142 PMID: 25822022

44. Margolis DM. Histone deacetylase inhibitors and HIV latency. Curr Opin HIV AIDS. 2011;6(1):25–9. https://doi.org/10.1097/COH.0b013e328341242d PMID: 21242890

45. Cillo AR, Sobolewski MD, Bosch RJ, Fyne E, Piatak M Jr, Coffin JM, et al. Quantification of HIV-1 latency reversal in resting CD4+ T cells from patients on suppressive antiretroviral therapy. Proc Natl Acad Sci U S A. 2014;111(19):7078–83. https://doi.org/10.1073/pnas.1402873111 PMID: 24706775

46. Rasmussen TA, Lewin SR. Shocking HIV out of hiding: where are we with clinical trials of latency reversing agents?. Curr Opin HIV AIDS. 2016;11(4):394–401. https://doi.org/10.1097/COH.0000000000000279 PMID: 26974532

47. Dufour C, Gantner P, Fromentin R, Chomont N. The multifaceted nature of HIV latency. The Journal of clinical investigation. 2021;130(7).

48. Adachi A, Gendelman HE, Koenig S, Folks T, Willey R, Rabson A, et al. Production of acquired immunodeficiency syndrome-associated retrovirus in human and nonhuman cells transfected with an infectious molecular clone. Journal of virology. 1986;59(2):284–91.